Journal of Catalysis 377 (2019) 629–637

Contents lists available at ScienceDirect

Journal of Catalysis

journal homepage: www.elsevier.com/locate/jcat

Lanthanum manganite-based perovskite as a catalyst for co-production of ethylene and hydrogen by ethane dehydrogenation

Xiaofeng Yang, Tong Wei, Bo Chi, Jian Pu, Jian Li *

Center for Fuel Cell Innovation, School of Materials Science and Engineering, Huazhong University of Science and Technology, Wuhan, Hubei 430074, China

ARTICLE INFO

Article history:
Received 5 April 2019
Revised 18 July 2019
Accepted 6 August 2019

Keywords:
Ni doped $LaMnO_3$
Exsolution
Dehydrogenation
Ethane
Ethylene

ABSTRACT

An A-site deficient and Ni-doped $LaMnO_3$ perovskite (LMN) is prepared and reduced in 5% H_2-N_2 at 800 °C for 1 (R-LMN) and 6 (ER-LMN) h for evaluation as catalysts for C_2H_6 dehydrogenation to co-produce C_2H_4 and H_2. The 1 h reduction causes the formation of Ni nanoparticles embedded in a perovskite substrate similar to LMN, but the excessive reduction for 6 h causes LMN decomposition to La_2O_3, MnO and Ni nanoparticles. The performance of the catalysts increases with increasing temperature. R-LMN demonstrates the highest performance among the catalysts studied, with 41.6% C_2H_6 conversion and 98.0% C_2H_4 selectivity at 750 °C; ER-LMN exhibits the lowest catalytic performance because of LMN decomposition. The performance of R-LMN is essentially stable during a 50 h test; and the slow growth of Ni nanoparticles slightly increases C_2H_6 conversion and decreases C_2H_4 selectivity due to the increase of the surface area of the Ni nanoparticles.

1. Introduction

Ethylene is a major intermediate for the production of numerous chemicals [1], and its global demand increases significantly every year. At present, ethylene is mainly produced commercially through steam cracking of naphtha or alkane feedstocks [1,2]. This process needs a tremendous amount of heat, which is provided by burning the undesired reaction products for the endothermic dehydrogenation reactions, resulting in severe emission of carbon dioxide (greenhouse gas) and nitrogen oxides (pollutants) [1]. Thus, developing a clean technical route for ethylene production is needed urgently.

Solid oxide fuel cells (SOFCs) are an electrochemical device that converts directly, efficiently and environmental-friendly the chemical energy stored in hydrocarbon fuels into electricity and heat. When a proton conducting electrolyte is used, the SOFC [3–8], which is accordingly designated as H-SOFC, can be used to co-produce electricity and ethylene, if C_2H_6 is used as the fuel and the anode is made to performs a dual-function of dehydrogenating C_2H_6 to ethylene (C_2H_4) and hydrogen (H_2) and electrochemically oxidizing only the formed H_2. Thus, the reactions occurring in the anode of the H-SOFC are

$$C_2H_6 = C_2H_4 + H_2 \text{ (dehydrogenation reaction)} \quad (1)$$

$$H_2 = 2H^+ + 2e^- \text{ (electrochemical reaction)} \quad (2)$$

The H^+ is transferred via the proton conducting electrolyte to the cathode where the H^+ reacts with oxygen ions O^{2-} to form H_2O; and the C_2H_4 can be collected at the anode exit without any CO_2 emission. Due to the consumption of the formed H_2 for power generation, thermodynamic equilibrium will not be a limit for reaction (1), which promotes the reaction towards forming the products continuously.

The state-of-the-art anode material for SOFCs is a cermet consisted of Ni and ceramic electrolyte (Ni-electrolyte). This cermet anode is highly chemically active for cracking hydrocarbons and electrocatalytically active for oxidizing H_2 [9,10], and therefore is not suitable for this purpose. In order to resolve this difficulty, Luo et al [11–17] investigated the possibility of co-production of C_2H_4 and electricity by C_2H_6 fueled H-SOFCs with Pt or Cr_2O_3-Cu as the anode, $BaCeO_3$ based proton conducting perovskite as the electrolyte and Pt as the cathode. The results showed that, at 750 °C, the conversion of C_2H_6 was in the range of few percent above 35%, the selectivity of C_2H_4 was lower than 90%, and the maximum power density achieved was usually below 175 mW cm^{-2}. If the H_2 produced were not consumed for power generation, the C_2H_6 conversion would be even lower. Therefore, these results indicate that both commercially available Pt and Cr_2O_3 are not an ideal material choice for the anode that is required to perform the dual functions of dehydrogenating C_2H_6 and oxidizing H_2. In addition, Pt has the potential of deeply cracking the unconverted C_2H_6 and hydrocarbons formed, causing carbon

* Corresponding author.
E-mail address: lijian@hust.edu.cn (J. Li).

https://doi.org/10.1016/j.jcat.2019.08.008
0021-9517/

deposition [15]. Furthermore, Cr_2O_3 is neither a good electronic nor a protonic conductor at the operating temperature. In order to facilitate the development of anode material for the co-production H-SOFC, it is proposed in this study to use a double-layer anode to avoid the necessity for one material to perform the dual-function role, as shown in Fig. 1. The outer layer catalyzes C_2H_6 dehydrogenation and the inner layer, as the functional anode, only oxidizes H_2 electrochemically. Based on this idea, the present study is undertaken to develop a catalyst for catalytic C_2H_6 dehydrogenation.

$LaMnO_3$ (LM)-based perovskites have long been used as cathode materials [18] for SOFCs and catalysts for CH_4 steam reforming [19] and partial oxidation [20]. Stimulated by these

previous studies, we have recently developed a perovskite oxide $La_{0.9}Mn_{0.8}Ni_{0.2}O_3$ (LMN), which is an A-site deficient LM with 20% Ni-doping, and used it as a catalyst for CO_2 dry reforming of CH_4 [21]. A-site deficiency (A/B < 1) promoted in-situ exsolution of Ni from the perovskite to form nano-sized Ni particles on the substrate [21–27], which resulted in high catalytic performance and carbon deposition resistance were achieved at 700 °C. Thus, in the present study, the LMN is explored for the first time as a catalyst for C_2H_6 dehydrogenation, and the related catalysis phenomena is also discussed.

2. Experimental

2.1. Materials synthesis and characterization

LMN powder was prepared by a sol-gel method with $La(NO_3)_3{\cdot}6H_2O$, $Ni(NO_3)_2{\cdot}6H_2O$ and $Mn(NO_3)_2{\cdot}4H_2O$ (Sino-Pharm chemical reagent) as precursors. The processing procedures were detailed in our previous work [21]. The prepared powder was ground and screened with a 100-mesh sieve, followed by a reduction process in 5% H_2-N_2 atmosphere at 800 °C for 1 (designated as R-LMN) and 6 h (excessive reduction, designated as ER-LMN), respectively, to form exsolved nano-sized Ni particles and examine the structure stability of the substrate.

The crystal structure and phase component of the LMN, R-LMN and ER-LMN were analyzed by X-ray diffraction (XRD, Shimadzu XRD-7000) in a range of the 2θ angle from 20 to 80° with Cu Kα radiation (λ = 1.5406 Å) at 40 kV, 30 mA and 10° min^{-1} scanning rate. The diffraction data LMN and R-LMN were refined by the EXPGUL software [28,29] using the space symmetry of $R\bar{3}C$ (ICSD No. 82315) and Pnma (ICSD No. 82227) [30] as the initial structure model, respectively, to determine the lattice parameters.

The surface chemistry of LMN and R-LMN were characterized by X-ray photoelectron spectroscopy (XPS) that was carried out on a Kratos Axis-Ultra DLD-600 W photoelectron spectrometer, using an Al monochromatic X-ray source. The C1s peak at 285 eV was used as reference to all binding energies. The obtained XPS spectra were fitted with a nonlinear Shirley-type background subtraction method. The position and area of the peaks were optimized by 80% Gaussian and 20% Lorentz functions.

The microstructure of the prepared catalysts before and after dehydrogenation tests was examined by a field emission scanning electron microscope (SEM, FEI Sirion 200) and a transmission electron microscope with an energy dispersive spectrometer (TEM, Tecnai G2-20). And the post-test R-LMN was further investigated by Raman spectrometry (RS, LabRAM HR800) at room temperature for carbon deposition estimation.

2.2. Dehydrogenation test

The test of C_2H_6 dehydrogenation was carried out in a fixed-bed quartz tube reactor (inner diameter = 6 mm) with and without (blank test) 0.2 g of the catalyst under atmospheric pressure at various temperatures between 625 and 750 °C. This temperature range was selected according to the fact that H-SOFCs are preferred

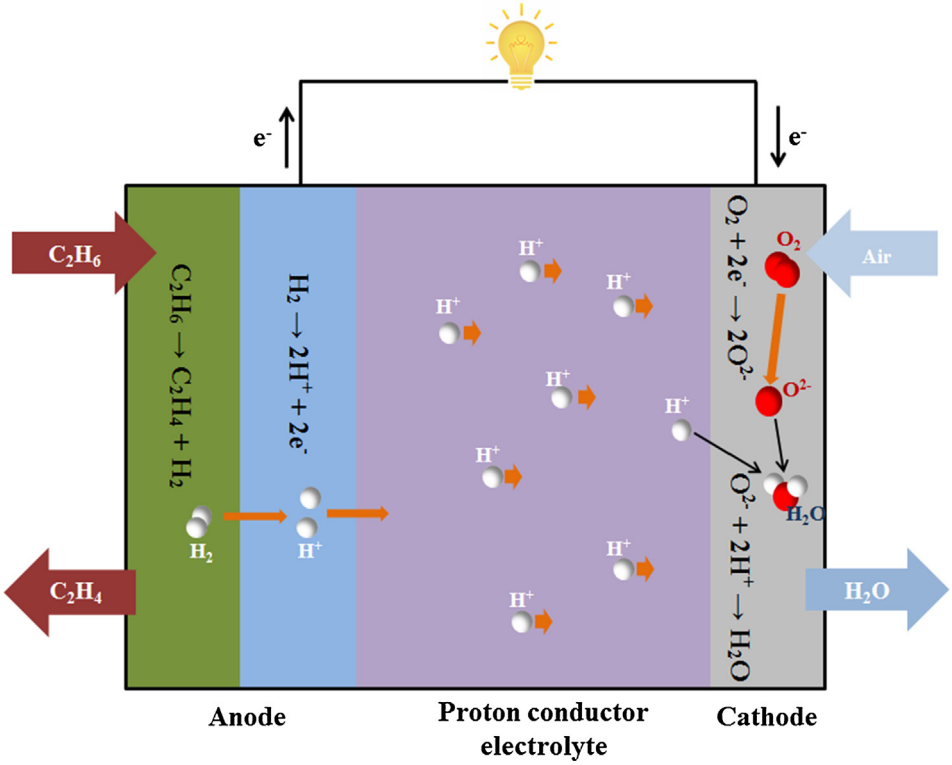

Fig. 1. Schematic diagram of H-SOFC for co-production of ethylene and electricity.

to be operated at these temperatures. C_2H_6 was continuously fed into the reactor at a flow rate of 50 ml min^{-1} (GHSV = 3×10^4 ml g^{-1} h^{-1}), and the gaseous product was carried by N_2 to a gas chromatograph (GC, GC4000 A, East & West (Beijing) Analytical Instruments) for composition analysis after steady-state operation was reached. The conversion of C_2H_6 (X_{C2H6}), selectivity of C_2H_4 (S_{C2H4}), CH_4 (S_{CH4}), CO_2 (S_{CO2}) and yield of C_2H_4 (Y_{C2H4}) were determined based on carbon conservation, respectively, by

$$X_{C2H6} = \frac{F_{C2H6(in)} - F_{C2H6(out)}}{F_{C2H6(in)}} \times 100\% \quad (3)$$

$$S_{C2H4} = \frac{F_{C2H4}}{F_{C2H6(in)} - F_{C2H6(out)}} \times 100\% \quad (4)$$

$$S_{CH4} = \frac{\frac{1}{2}F_{CH4}}{F_{C2H6(in)} - F_{C2H6(out)}} \times 100\% \quad (5)$$

$$S_{CO2} = \frac{\frac{1}{2}F_{CO2}}{F_{C2H6(in)} - F_{C2H6(out)}} \times 100\% \quad (6)$$

$$Y_{C2H4} = X_{C2H6} \times S_{C2H4} \times 100\% \quad (7)$$

And the catalytic activity is characterized by specific production rate of C_2H_4 (r_{C2H4}), determined by

$$r_{C2H4} = \frac{F_{C2H4}}{M_{catalyst}} \quad (8)$$

where the $F_{C2H6(in)}$, $F_{C2H6(out)}$, F_{C2H4}, F_{CH4} and F_{CO2} represent the mole flow velocity of each component during the test, and the $M_{catalyst}$ represent the mass of the catalyst. The ratio $\frac{r_{C2H4(catalyst)}}{r_{C2H4(blank)}}$ was used to characterize the effect of catalyst on the dehydrogenation of ethane to ethylene.

3. Results

3.1. Phase and microstructure

Fig. 2 shows the XRD pattern of as-prepared LMN, R-LMN and ER-LMN. Single phase LMN was formed with a perovskite structure similar to that of LM (PDF file # 89-2471), suggesting that 20% of Ni was fully doped into the structure of LM (Fig. 2a). By a reduction process in 5% H_2-N_2 atmosphere at 800 °C for 1 h (R-LMN), part of Ni in LMN was exsolved as metallic Ni from the substrate still maintained in perovskite structure (Fig. 2a). By closely examining the diffraction patterns of LMN and R-LMN, it is noted that some diffraction peaks of LMN were split into two peaks, and the corresponding peaks of R-LMN remained as single peaks. This suggests that the crystal structures of LMN and the substrate of R-LMN were slightly different due to decreased degree of A-site deficiency in the substrate caused by Ni exsolution out of LMN lattice, although they both had a perovskite structure. The Rietveld refinement results, as listed in Table 1, indicate that the LMN possessed a rhombohedral structure ($R\bar{3}C$) and the substrate in R-LMN possessed an orthorhombic structure (Pnma) due to lattice shuffling accompanying Ni exsolution. However, excessively reducing the LMN under the same environment for 6 h (ER-LMN) led to the decomposition of LMN to La_2O_3, MnO and Ni (Fig. 2b). The fact that the intensity of Ni peaks in the diffraction pattern for R-LMN (190 counts) is lower than that for ER-LMN (293 counts) may imply qualitatively that the Ni in R-LMN was not completely exsolved during the 1 h reduction process.

Fig. 3 shows the microstructure of as-prepared LMN, R-LMN and ER-LMN. It is observed that the morphology of R-LMN remained similar to that of LMN (Fig. 3a), and the uniformly distributed nano-sized Ni particles (averagely ~20 nm) were formed by exsolution and partially embedded in the perovskite substrate (Fig. 3b and c). But the morphology of ER-LMN was entirely changed with slightly larger and round Ni particles sporadically spotted on the decomposed substrate (Fig. 3d). According to the BET measurement,

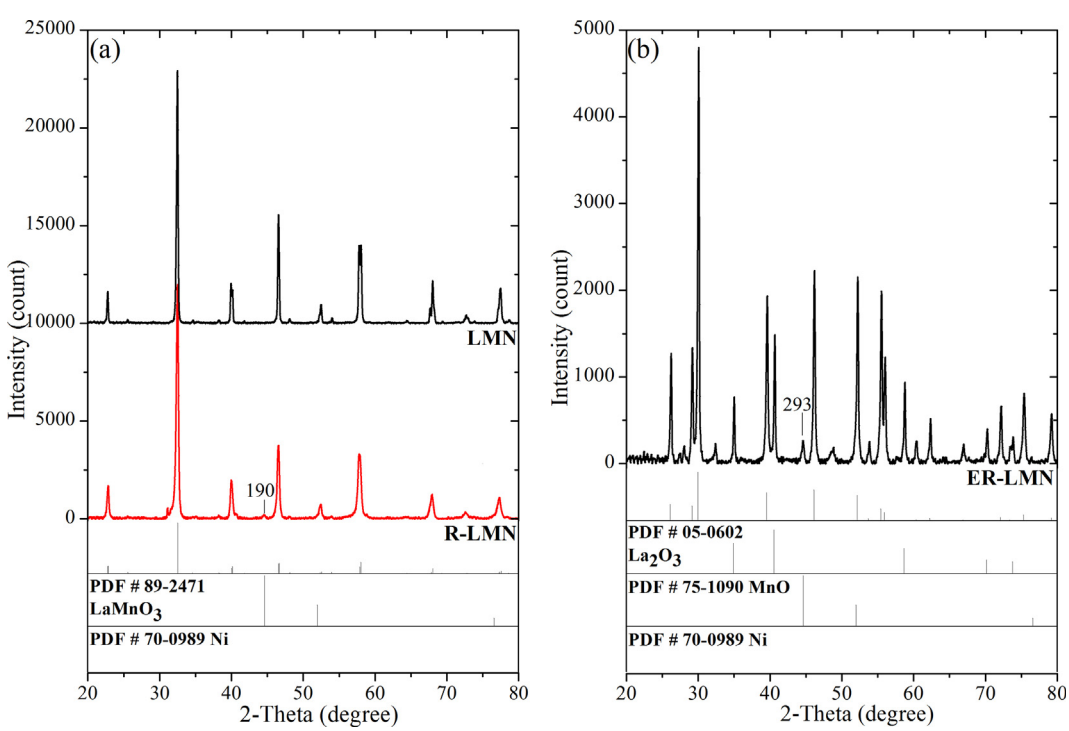

Fig. 2. XRD pattern of as-prepared (a) LMN, R-LMN and (b) ER-LMN.

Table 1
Unit cell parameters of LMN and R-LMN determined by the Rietveld refinement.

Sample	Space group	a (Å)	b (Å)	c (Å)	V (Å^3)
LMN	$R\bar{3}C$	5.5124	–	13.3172	350.44
R-LMN	Pnma	5.5051	7.7977	5.5437	237.98

the specific surface area of R-LMN (10.32 $m^2\,g^{-1}$) was slightly larger than that of LMN (7.28 $m^2\,g^{-1}$) due to the contribution of the exsolved nano-sized Ni particles.

3.2. Surface chemistry

LMN and R-LMN were subjected to XPS analysis to understand their surface chemistry; the result is shown in Fig. 4. The peaks of Ni, La, Mn and O were detected, together with that of C (peak C 1s at ~285 eV) due to carbonate contamination on the surface (Fig. 4a) [31]. The peak of Mn 2p (Fig. 4b) in the binding energy range between 640.6 and 640.9 eV was characterized to Mn^{3+}, and that between 641.8 and 642.2 eV was assigned to Mn^{4+}. According to area of the peak, the ratio of surface Mn^{4+} to Mn^{3+} was estimated to be 0.756 for R-LMN, which suggests that approximately 43% of Mn on the surface of R-LMN was in the oxidation state of valence + 4.

3.3. Catalytic activity

The LMN, R-LMN and ER-LMN were evaluated as the catalysts for C_2H_6 dehydrogenation at various temperatures between 625 and 750 °C. The conversion of C_2H_6 and selectivity of C_2H_4, CH_4 and CO_2 were determined by Eqs. (3)–(6) using the composition of the product gas measured by GC. Fig. 5 shows the average value for a period of 90 min after the reaction was stabilized. It is seen that the C_2H_6 conversion by all the catalysts increased with the increase of testing temperature. However, at temperatures above 675 °C, the conversion by R-LMN was obviously higher than those by LMN and ER-LMN, and the conversion by ER-LMN was the lowest. At 750 °C, the conversion by R-LMN was 41.6%, while that by LMN and ER-LMN was 36.9 and 33.6%, respectively. Unlike their behavior in conversion, C_2H_4 selectivity of the catalysts studied was not as sensitive to the testing temperature as the conversion, it only decreased slightly from 100 to around 98% in the temperature range between 625 and 750 °C for all the three catalysts, accompanied with the formation of small amounts of CH_4 and CO_2. According to Eq. (7), the C_2H_4 yield of R-LMN was determined as 40.8% at 750 °C. In order to further explore the effect of R-LMN on dehydrogenation of C_2H_6, the conversion of C_2H_6 and selectivity of C_2H_4 of the blank test and the ratio $r_{C2H4(R\text{-}LMN)}/r_{C2H4(blank)}$ (using the data determined by Eq. (8) and listed in Table 2) are shown in Fig. 6. It is clear that the reaction of C_2H_6 dehydrogenation occurred without R-LMN due to thermal crack; however, the production rate was significantly increased by the presence of R-LMN, and the effect of R-LMN was enhanced with the increase of testing temperature.

3.4. Performance durability

Since the R-LMN showed the best initial performance among the three catalysts studied, it was subjected to a long-term test for 50 h at 750 °C for evaluating its performance durability, the

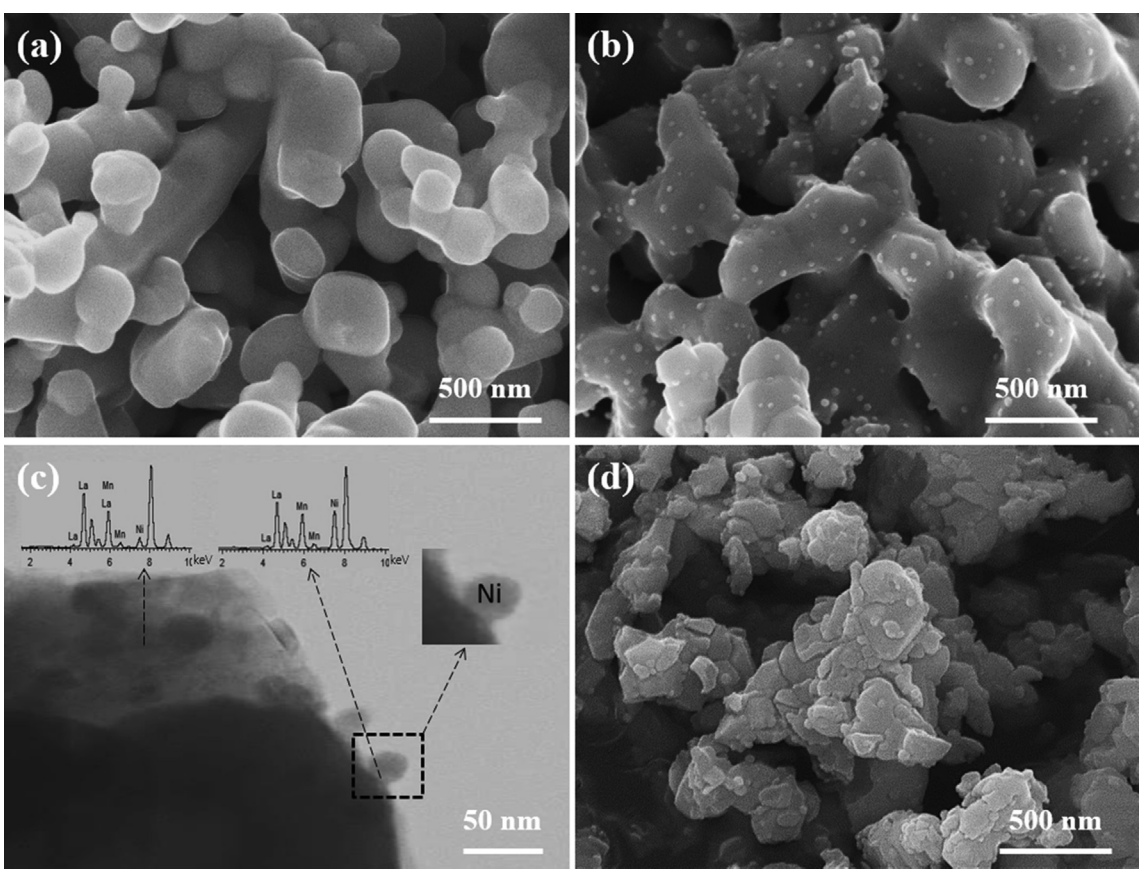

Fig. 3. Microstructure of as-prepared (a) LMN, (b, c) R-LMN and (d) ER-LMN.

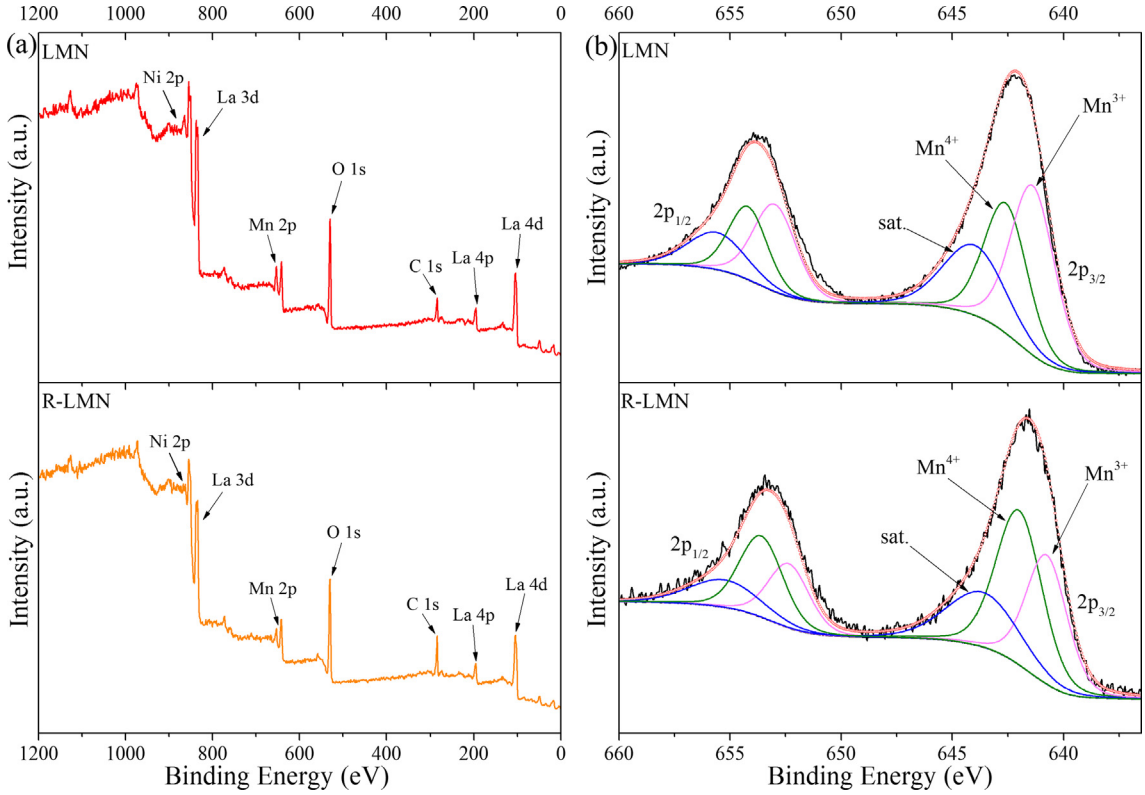

Fig. 4. Representative (a) and Mn (b) XPS spectra of LMN and R-LMN.

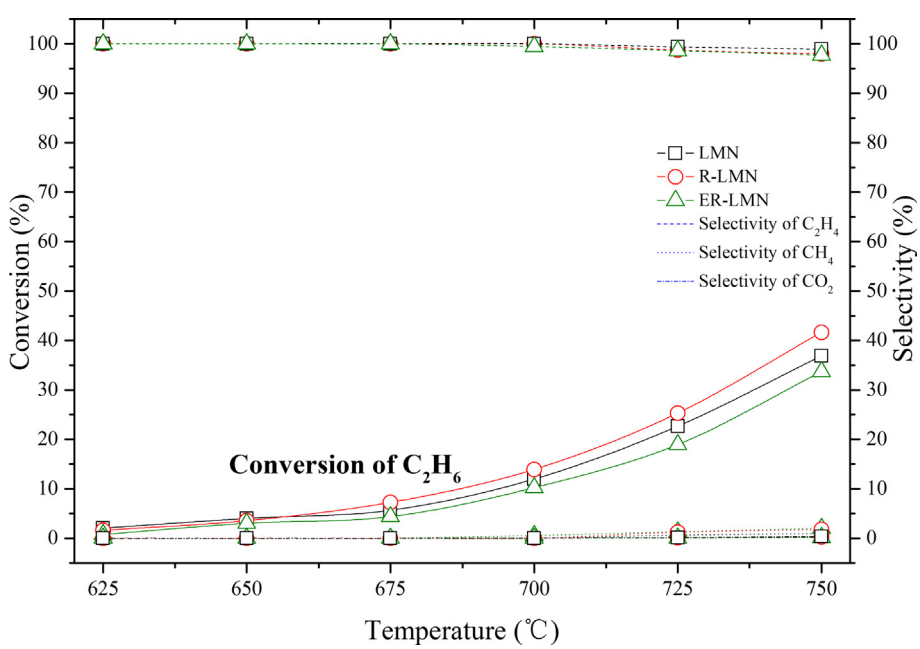

Fig. 5. Performance of LMN, R-LMN and ER-LMN for C_2H_6 dehydrogenation at various temperatures (testing conditions: N_2:C_2H_6 = 1:1, flow rate = 100 ml min^{-1}, 0.2 g catalysts, GHSV = 3×10^4 ml g^{-1} h^{-1}).

result is shown in Fig. 7. During the 50 h test, the performance of R-LMN was essentially stable, and the conversion and selectivity slightly increased and decreased, respectively, after around 30 h of test. At the end of 50 h test, the conversion was 43.4% and the selectivity was 97.3%. The R-LMN after the performance durability test was analyzed by Raman spectrometry to determine whether carbon deposition happened. The result is shown in Fig. 8, which indicates that carbon deposition did not occur in the R-LMN during the 50 h test, as the characteristic peaks at 1350 (D-peak) and 1580 cm^{-1} (G-peak), which are for disordered and graphitic

Table 2
The dependence of the specific production rate of C_2H_4 with and without R-LMN on temperature.

T(°C)	$r_{C2H4(blank)}$ (μmol s^{-1} g^{-1})	$r_{C2H4(R-LMN)}$ (μmol s^{-1} g^{-1})
625	1.09	1.26
650	1.68	2.75
675	2.74	5.77
700	4.40	11.16
725	7.35	20.56
750	11.59	33.14

Reaction conditions: N_2:C_2H_6 = 1:1, flow rate = 100 ml min^{-1}, 0.2 g catalysts, GHSV = 3 × 10^4 ml g^{-1} h^{-1}.

carbon, respectively, were not present. Fig. 9 shows the microstructure and XRD pattern of the R-LMN tested for 50 h. It appears that the exsolved Ni particles grew slightly (~35 μm) without significantly increasing the particle number. This observation is consistent with that reported previously by Irvine et al. [27] and Tong et al. [21], and may suggest that the process of Ni nucleation was completed after the reduction in 5% H_2-N_2 atmosphere at 800 °C for 1 h, and the process of Ni particle growth proceeded slowly during the test at 750 °C until all the Ni doped was entirely exsolved. The slow slight increase in the conversion and decrease in selectivity may be caused by the increase of the surface area of the exsolved Ni particles.

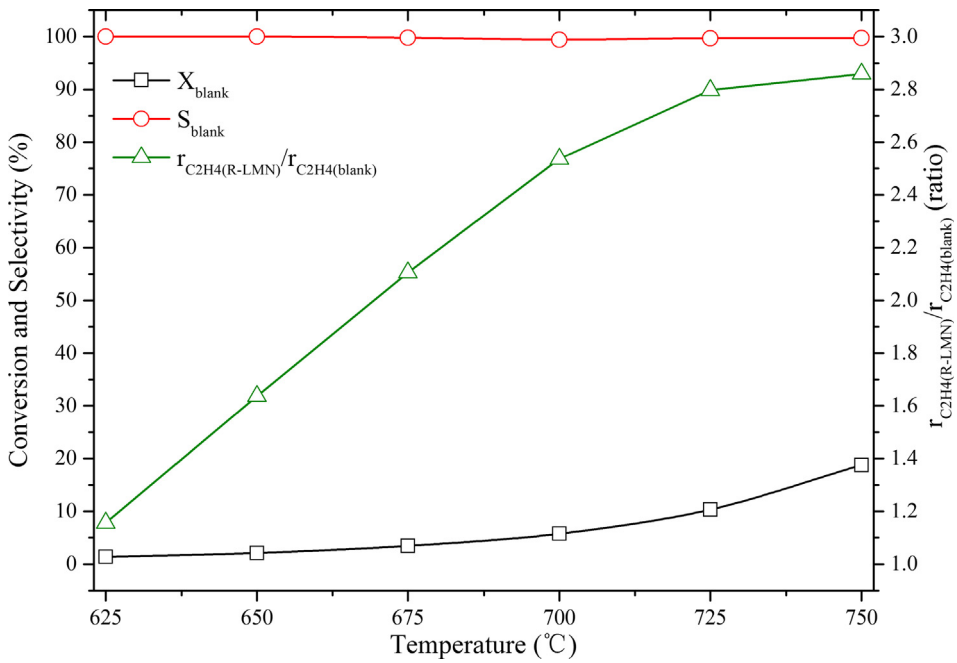

Fig. 6. Blank test result and the effect of R-LMN and temperature on the specific production rate of C_2H_4.

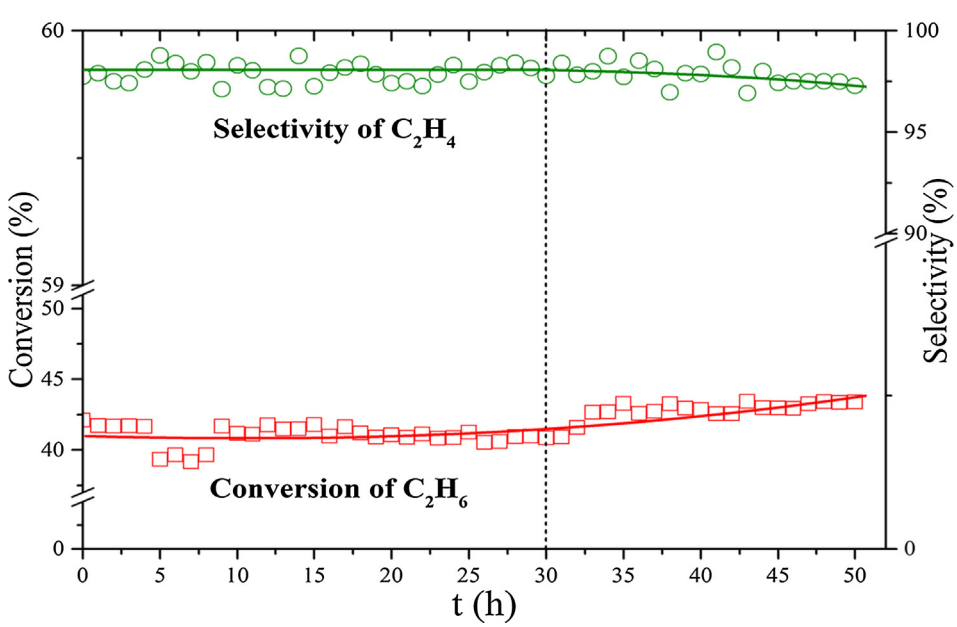

Fig. 7. Performance durability of R-LMN for C_2H_6 dehydrogenation at 750 °C (testing conditions: N_2:C_2H_6 = 1:1, flow rate = 100 ml min^{-1}, 0.2 g catalysts, GHSV = 3 × 10^4 ml g^{-1} h^{-1}).

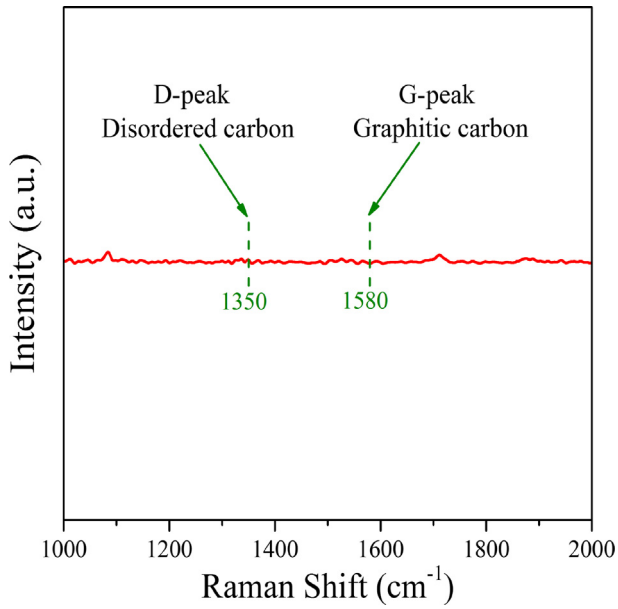

Fig. 8. Raman spectrum of R-LMN tested for 50 h at 750 °C.

4. Discussion

With Ni (+2 valence) doping, the electrical neutrality of LMN is expected to be maintained by the oxidation of some Mn^{3+} ions to Mn^{4+} and also the formation of oxygen vacancies in LMN. In fact, the results of XPS demonstrated the presence of Mn^{4+} ions (~43% shown in Fig. 4) and oxygen vacancies [21] on the surface of R-LMN. Based on these experimental results, it is proposed that C_2H_6 dehydrogenation process on the surface of LMN catalyst may proceed with the following steps, as shown in Fig. 10. The first step is the adsorption of C_2H_6 on oxygen vacancy sites [O] near Mn^{4+} ions. The second step is that the activation of C—H bonds by oxygen vacancies, resulting in the breakage of C—H bonds and the formation of C_2H_4, which was adsorbed on the oxygen vacancy sites, and two H^+ ions, which were associated with nearby lattice oxygen ions (OH^-). The formal oxidation state of carbon in C_2H_6 and C_2H_4 are −3 and −2, respectively, the two excess electrons originally from H reduce Mn^{4+} to Mn^{3+} ions. The third step is the desorption of C_2H_4 from the oxygen vacancy sites and the reduction of the nearby OH^- hydroxides by obtaining electrons from Mn^{3+} ions to release of H atoms to form H_2, and in the meantime, Mn^{3+} ions are re-oxidized to form Mn^{4+} ions. After these three steps, the LMN surface resumes its original state. This catalytic cycle is repeated to continuously dehydrogenate C_2H_6 to C_2H_4 and H_2.

Once Ni nano particles are formed by exsolution on the surface of LMN substrate, Ni content in the substrate is reduced, and accordingly the catalytic activity of the substrate decreases due to the decrease of Mn^{4+} ions and oxygen vacancies. However, the Ni nano particles formed will play a significant catalytic role for C_2H_6 dehydrogenation. It is well known that Ni is an excellent catalyst for activation and breakage of C—H and C—C bonds. Therefore, the presence of Ni nano particles enhances the catalytic activity for C_2H_6 dehydrogenation with a catalytic process shown

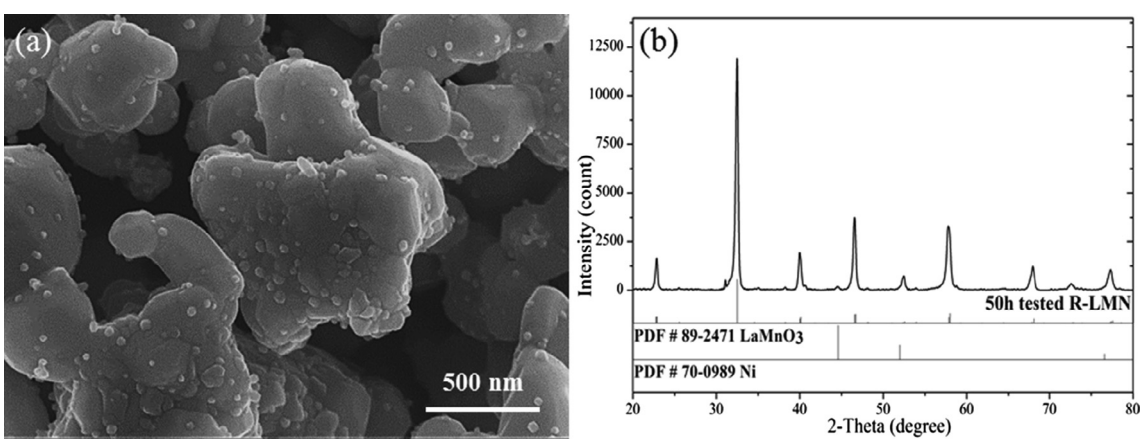

Fig. 9. Microstructure (a) and XRD pattern (b) of R-LMN tested for 50 h.

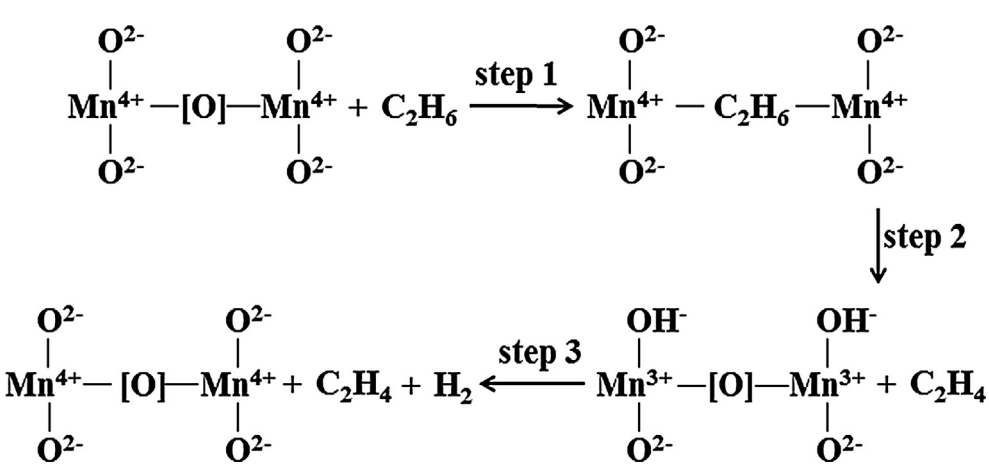

Fig. 10. Schematic diagram of C_2H_6 dehydrogenation process catalyzed by LMN.

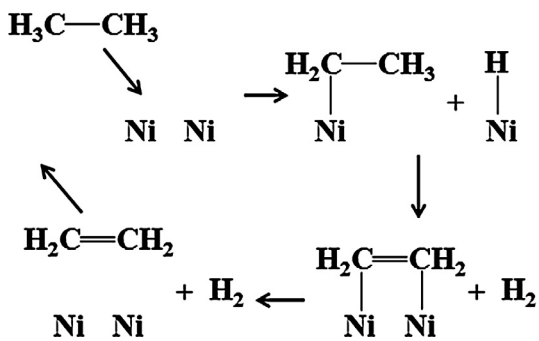

Fig. 11. Schematic diagram of C_2H_6 dehydrogenation process catalyzed by metallic Ni.

in Fig. 11, which is similar with the catalytic process of Pt [32]. With the catalytic assistance of the Ni nano particles, the adsorbed C_2H_6 with a single carbon-carbon bond will readily release H_2 and form C_2H_4 with a double carbon-carbon bond. It is because of the high catalytic activity of the Ni nano particles that the performance of R-LMN was higher than that of LMN for C_2H_6 dehydrogenation (Fig. 5). In the ER-LMN, the original substrate LMN was completely decomposed to La_2O_3, MnO and Ni. La_2O_3 and MnO are not as catalytically active as perovskite LMN, and some of the Ni particles was covered by La_2O_3 and MnO and not exposed to C_2H_6 gas. Therefore, the performance of ER-LMN for C_2H_6 dehydrogenation was the lowest among the three catalysts (Fig. 5).

As mentioned earlier, in the 50 h dehydrogenation test of R-LMN, C_2H_6 conversion increased slightly and C_2H_4 selectivity decreased somewhat after 30 h of testing. On the basis of the discussion above, this phenomenon can be understood. The R-LMN was obtained by reducing the LMN at 800 °C in 5% H_2-N_2 atmosphere for 1 h. Only part of the doped Ni was exsolved in the pre-reduction process. During the long-term test, the R-LMN was exposed constantly to a reducing (low oxygen partial pressure) atmosphere consisting mostly of the unconverted C_2H_6 and the formed C_2H_4 and H_2. Under this circumstance, the Ni remaining in the substrate would be exsolved gradually with time, resulting in the continuous growth of the Ni nano particles rather than the formation of "new" Ni nano particles (Fig. 9). Thus the surface area of the exsolved Ni nano particles would increase with time, promoting the process of C_2H_6 conversion. Since the growth of Ni nano particles was slow, the increase of C_2H_6 conversion was observed only after 30 h of testing, which was accompanied with insignificant decrease of C_2H_4 selectivity possibly due to the formation of some CH_4 as the Ni catalyst is very active for breaking the carbon-carbon bonds. On the basis of these analyses, it becomes clear that for the development of highly efficient LMN catalyst for C_2H_6 dehydrogenation, the amount of Ni doping needs to be optimized to balance the amount of Ni that remains in the perovskite substrate against the amount of Ni that is exsolved on the perovskite substrate in the form of Ni nano particles.

5. Conclusions

LMN, R-LMN and ER-LMN were evaluated as catalysts for C_2H_6 dehydrogenation. Based on the results obtained, the following conclusions can be made.

(1) Reducing the 20% Ni doped perovskite LMN in a 5% H_2-N_2 atmosphere at 800 °C for 1 h results in the formation of nano-sized Ni particles, which are partially embedded in the substrate with a perovskite structure, which contains less amount of Ni than as-prepared LMN. However, when excessively reduced under the same conditions for 6 h, LMN decomposes to La_2O_3, MnO and dispersed Ni nano particles.

(2) Catalytic performance of all the three catalysts increases with the increase of testing temperature from 625 to 750 °C. R-LMN out-performances LMN due to the exsolution of Ni nano particles on the perovskite substrate in R-LMN; and ER-LMN exhibits the lowest performance because of the decomposition of LMN. The catalytic activity of LMN is probably associated with the presence of Mn^{4+} ions and oxygen vacancies.

(3) Catalytic performance of R-LMN at 750 °C is essentially stable without carbon deposition, and C_2H_6 conversion and C_2H_4 selectivity are approximately on the level of 43% and 98%, respectively. The slow growth of Ni nano particles caused by further exsolution during the test slightly increases the conversion and decreases the selectivity, which suggests that, to develop a high efficiency C_2H_6 dehydrogenation catalyst, it is necessary to optimize of Ni content in the doped LMN to balance of the amount of Ni that is exsolved on the substrate against the amount of Ni that remains in the substrate.

Acknowledgements

This research was financially supported by the National Key Research & Development Project-International Cooperation Program (2016YFE0126900), National Natural Science Foundation of China (U1601207, 51672095). SEM, XRD and Raman spectrometry characterizations were assisted by the Analytical and Testing Center of Huazhong University of Science and Technology and the State Key Laboratory of Material Processing and Die & Mold Technology. The authors acknowledge Prof. Zhidong Xiang of Wuhan University of Science and Technology for proofreading the manuscript.

References

[1] A.S. Bodke, D.A. Olschki, L.D. Schmidt, E. Ranzi, Science 285 (1999) 712–715, https://doi.org/10.1126/science.285.5428.712.
[2] E. Heracleous, A.A. Lemonidou, J. Catal. 270 (2010) 67–75, https://doi.org/10.1016/j.jcat.2009.12.004.
[3] S.M. Haile, Acta Mater. 51 (2003) 5981–6000, https://doi.org/10.1016/j.actamat.2003.08.004.
[4] S.W. Tao, J.T.S. Irvine, Adv. Mater. 18 (2006) 1581–1584, https://doi.org/10.1002/adma.200502098.
[5] C.D. Zuo, S.W. Zha, M.L. Liu, M. Hatano, M. Uchiyama, Adv. Mater. 18 (2006) 3318–3320, https://doi.org/10.1002/adma.200601366.
[6] A. Tomita, K. Tsunekawa, T. Hibino, S. Teranishi, Y. Tachi, M. Sano, Solid State Ion. 177 (2006) 2951–2956, https://doi.org/10.1016/j.ssi.2006.08.031.
[7] S. Barison, M. Battagliarin, T. Cavallin, L. Doubova, M. Fabrizio, C. Mortalo, S. Boldrini, L. Malavasi, R. Gerbasi, J. Mater. Chem. 18 (2008) 5120–5128, https://doi.org/10.1039/b808344d.
[8] Y. Guo, Y. Lin, R. Ran, Z. Shao, J. Power Sources 193 (2009) 400–407, https://doi.org/10.1016/j.jpowsour.2009.03.044.
[9] J.W. Fergus, Solid State Ion. 177 (2006) 1529–1541, https://doi.org/10.1016/j.ssi.2006.07.012.
[10] C.W. Sun, U. Stimming, J. Power Sources 171 (2007) 247–260, https://doi.org/10.1016/j.jpowsour.2007.06.086.
[11] S.Y. Wang, J.L. Luo, A.R. Sanger, K.T. Chuang, J. Phys. Chem. C 111 (2007) 5069–5074, https://doi.org/10.1021/jp066690w.
[12] X.Z. Fu, J.L. Luo, A.R. Sanger, N. Danilovic, K.T. Chuang, Chem. Commun. 46 (2010) 2052–2054, https://doi.org/10.1039/b926928b.
[13] X.Z. Fu, J.L. Luo, A.R. Sanger, N. Luo, K.T. Chuang, J. Power Sources 195 (2010) 2659–2663, https://doi.org/10.1016/j.jpowsour.2009.10.069.
[14] X.Z. Fu, J.L. Luo, A.R. Sanger, Z.R. Xu, K.T. Chuang, Electrochim. Acta 55 (2010) 1145–1149, https://doi.org/10.1016/j.electacta.2009.10.010.
[15] Z.C. Shi, J.L. Luo, S.Y. Wang, A.R. Sanger, K.T. Chuang, J. Power Sources 176 (2008) 122–127, https://doi.org/10.1016/j.jpowsour.2007.10.056.
[16] X.Z. Fu, X.X. Luo, J.L. Luo, J. Power Sources 196 (2011) 1036–1041, https://doi.org/10.1016/j.jpowsour.2010.08.043.
[17] X.Z. Fu, J.Y. Lin, S.H. Xu, J.L. Luo, Phys. Chem. Chem. Phys. 13 (2011) 19615–19623, https://doi.org/10.1039/c1cp22837d.

[18] S.P. Jiang, J. Mater. Sci. 43 (2008) 6799–6833, https://doi.org/10.1007/s10853-008-2966-6.
[19] A. Evdou, V. Zaspalis, L. Nalbandian, Int. J. Hydrogen Energy 33 (2008) 5554–5562, https://doi.org/10.1016/j.ijhydene.2008.06.036.
[20] S. Ponce, M.A. Peña, J.L.G. Fierro, Appl. Catal. B 24 (2000) 193–205, https://doi.org/10.1016/S0926-3373(99)00111-3.
[21] T. Wei, L.C. Jia, H.Y. Zheng, B. Chi, J. Pu, J. Li, Appl. Catal. A – Gen. 564 (2018) 199–207, https://doi.org/10.1016/j.apcata.2018.07.031.
[22] J.T.S. Irvine, D. Neagu, M.C. Verbraeken, C. Chatzichristodoulou, C. Graves, M.B. Mogensen, Nat. Energy 1 (2016) 15014, https://doi.org/10.1038/NENERGY.2015.14.
[23] B. Hua, M. Li, Y.F. Sun, J.H. Li, J.L. Luo, ChemSusChem 10 (2017) 3333–3341, https://doi.org/10.1002/cssc.201700936.
[24] O. Kwon, S. Sengodan, K. Kim, G. Kim, H.Y. Jeong, J. Shin, Y.W. Ju, J.W. Han, G. Kim, Nat. Commun. 8 (2017) 15967, https://doi.org/10.1038/ncomms15967.
[25] D. Neagu, E.I. Papaioannou, K.W.R. Wan, D.N. Miller, B.J. Murdoch, H. Ménard, A. Umar, A.J. Barlow, P.J. Cumpson, J.T.S. Irvine, Nat. Commun. 8 (2017), https://doi.org/10.1038/s41467-017-01880-y.
[26] D. Neagu, G. Tsekouras, D.N. Miller, J.T. Irvine, Nat. Chem. 5 (2013) 916–923, https://doi.org/10.1038/NCHEM.1773.
[27] D. Neagu, T.S. Oh, D.N. Miller, H. Ménard, S.M. Bukhari, S.R. Gamble, R.J. Gorte, J.M. Vohs, J.T. Irvine, Nat. Commun. 6 (2015) 8120, https://doi.org/10.1038/ncomms9120.
[28] A.C. Larson, R.B.V. Dreele, Los Alamos National Laboratory Report LAUR 86 (1994) 748.
[29] B.H. Toby, J. Appl. Crystallogr. 34 (2001) 210–213, https://doi.org/10.1107/S0021889801002242.
[30] P. Norby, I.G.K. Andersen, E.K. Andersen, N.H. Andersen, J. Solid State Chem. 119 (1995) 191–196, https://doi.org/10.1016/0022-4596(95)80028-N.
[31] Y.N. Lee, R.M. Lago, J.L.G. Fierro, V. Cortés, F. Sapiña, E. Martınez, Appl. Catal. A Gen. 207 (2001) 17–24, https://doi.org/10.1016/S0926-860X(00)00610-4.
[32] V. Galvita, G. Siddiqi, P.P. Sun, A.T. Bell, J. Catal. 271 (2010) 209–219, https://doi.org/10.1016/j.jcat.2010.01.016.